Linear Instability with Ekman and Interior Friction. Part I: Quasigeostrophic Eigenanalysis

RICHARD GROTJAHN

Department of Land, Air and Water Resources, University of California, Davis, Davis, California

MIN CHEN

Environmental Health and Sciences Laboratory, Mobil Oil Corporation, Princeton, New Jersey

JOSEPH TRIBBIA

National Center for Atmospheric Research, Boulder, Colorado

(Manuscript received 2 August 1993, in final form 8 August 1994)

ABSTRACT

The eigenvalue problems for the original Eady model and a modified Eady model (the G model) are examined with no friction, Ekman friction only, and both Ekman and interior friction. When both Ekman and interior friction are included in the models, normal modes show little additional change when compared to the case with Ekman friction only, whereas the relevant "continuum modes" have large negative growth rates. Interior friction has a much greater effect on the continuum modes than on the normal modes because inviscid continuum modes have a delta-function vertical profile of potential vorticity q. In contrast, normal modes have much smoother profiles of q in the interior. Streamfunction profiles for the continuum modes are notably different in the two models. The continuum modes in the more realistic G model have sharp peak amplitudes that are not as broad in the vertical as in the Eady model.

1. Introduction

Charney (1947) and Eady (1949) are pioneering theoretical studies of linear baroclinic instability. The Eady and Charney models have become the basis of most investigations of baroclinic instability, including the results discussed here.

Eigensolutions for these models exist in two general categories. One group is labeled *normal modes,* which can be exponentially growing. The other group is called *continuum modes;* these modes are neutral in the inviscid case, and their structure and phase speed are tied to the basic flow, U. When we solve the inviscid eigenvalue problems using N discrete levels in the vertical, two normal modes and $N - 2$ neutral modes occur. The neutral modes are analogous to the continuum modes, and we refer to these modes as "continuum modes" hereafter. Analogous normal and continuum modes also are found when friction is added, though in general the continuum modes are no longer neutral. The structure, size, growth rate, and phase speed of the exponentially growing normal modes are similar to the observed, *developing* frontal cyclones. Consequently, most linear instability studies ignore continuum modes and focus on the properties of the normal-mode solutions.

The Eady model has been improved upon in numerous studies of baroclinic instability. Grotjahn (1980) modifies the Eady model to include compressibility, variable Coriolis parameter, and more realistic vertical profiles of zonal-mean velocity and static stability. This modified Eady model is hereafter called the G model. Unlike the Eady model, the G model does not have a short-wave cutoff to the growth rate, so all wavelengths are unstable in the inviscid case. The most unstable wavelength is around 4500 km, which is comparable to Eady's result. We use the G model to explore how results found with the Eady model appear in a model having fewer dynamical restrictions.

2. The motivation for examining friction

Friction occurs at the boundary of the atmosphere with land or ocean (boundary friction) and inside the atmosphere itself (interior friction). Boundary friction may have a more significant impact on atmospheric dynamics because it is in general considerably larger than interior friction. Holopainen (1961) addressed this concern by including Ekman friction in the Phillips

Corresponding author address: Prof. Richard Grotjahn, Dept. of Land, Air and Water Resources, University of California, Davis, Rm. 151, Hoagland Hall, Davis, CA 95616.

© 1995 American Meteorological Society

Unauthenticated | Downloaded 05/29/24 05:02 AM UTC

(1954) two-layer model and concluded that friction reduced the growth rate of the perturbation field except within two narrow wavebands where waves (neutral normal modes) that were marginally stable under inviscid conditions were destabilized. Later, Romea (1977) obtained similar results in a nonlinear version of a similar model. Barcilon (1964) and Williams and Robinson (1974) employed an Eady-type model, which included Ekman pumping at both the top and bottom boundaries or only at the bottom. They found that the single Ekman layer at the bottom had a destabilizing effect on the dynamics of short waves. With top and bottom Ekman layers, the growth rates of the perturbation declined, as expected, producing short- and long-wave cutoffs. Card and Barcilon (1982) used the Charney model with the inclusion of Ekman pumping at the bottom boundary. These results demonstrated that Ekman pumping at the lower boundary led to a significant reduction in instability for disturbances of all wavelengths.

Farrell (1985) finds that Ekman friction strongly dampens the normal modes in his model. Farrell only uses a single meridional wavenumber corresponding to a channel width of 1500 km. Lin and Pierrehumbert (1988, hereafter LP) find that such a narrow channel forces all solutions to have large absolute wavenumber leading to large vertical vorticity component and therefore large Ekman friction. For a larger channel width, LP find the instability to be present even with a ν that is 10 times larger than Farrell's. Further, LP state that the instability can be eliminated only with a combination of strong Ekman friction and weak large-scale wind shear. Lin and Pierrehumbert discuss estimates of Ekman friction based on a boundary layer model and conclude that, over the ocean, Ekman friction could reduce the growth rate of the most unstable mode as much as a factor of 2 but would not eliminate the instability.

An Ekman layer has a strong effect upon the normal modes and little effect upon most continuum modes. The reason for this difference is because the normal modes have potential vorticity q at the vertical boundaries. Bretherton (1966) showed that the northward geostrophic eddy flux of potential vorticity ($v'q'$) for a normal mode in the Eady model is solely at the boundaries. The $v'q'$ flux is balanced by a heat flux at z_b (bottom) and/or z_t (top) since the conservation of potential temperature equation is used as the vertical boundary condition. Therefore, Ekman friction, which creates a "pumping" term in the boundary conditions, has a large effect on the normal modes. On the other hand, continuum modes do not have smooth profiles of q. Pedlosky (1987) shows that the q for continuum modes has a shape like a delta function when plotted against the vertical dimension z. This delta-function q for a continuum mode reaches a maximum near the steering level for that mode, which is somewhere in the interior of the domain. Hence, Ekman friction has little effect on most continuum modes.

Interior dissipation also affects continuum and normal modes differently. As noted by Miles (1965), internal dissipation reflecting heat conduction gives interior terms that are approximately proportional to the vertical second derivative of q. Viscosity coefficients for interior friction are small, so interior friction may be neglected when one deals with the normal modes since those modes have smooth vertical profiles of q. Realistic total flows would, in general, have smooth profiles, and interior viscosity may be neglected in those cases as well. This scaling argument probably accounts for the lack of interior friction in linear instability model studies done so far. On the other hand, initial conditions that optimize nonmodal growth may have very sharp vertical tilts, and it is less clear that interior viscosity may be neglected. If the sharp tilt is confined to a narrow range of height, such an optimal structure is well approximated by just a few continuum modes. Since interior profiles of q for continuum modes are very much sharper than for normal modes, even a small amount of interior friction has a drastic effect upon this portion of the spectrum. Therefore, adding Ekman friction without interior friction may spuriously favor continuum modes.

The vertical structure of discrete approximations to continuum modes has not been presented in the literature except for the simplest models. This paper describes those eigenfunctions for a more realistic model and points out key ways that they differ from the Eady model. The structures of the discretized continuum modes are quite different, and that may impact other papers in the literature that invoke continuum modes for various reasons (such as nonmodal growth).

This paper describes numerical experiments using the eigenvalue formulation of the Eady and the G models. Experiments are performed under three conditions: 1) inviscid (no friction); 2) viscous with only Ekman friction; and 3) viscous with both Ekman and interior friction. The results should enable us to answer the following questions: What do discrete approximations to continuum modes look like in more realistic models? How much does a small but consistent amount of interior viscosity damp such modes? How does the damping of such modes compare with the normal-mode growth? How do the structures of discretized continuum and normal modes change in response to each type of friction?

3. Model description

a. Formulation of the eigenvalue problem

The model is developed and described in Grotjahn (1979, 1980). The G model modifies the Eady (1949) model several ways. Compressibility and linear variation of the Coriolis parameter are included, similar to

Unauthenticated | Downloaded 05/29/24 05:02 AM UTC

Green (1960). However, the density variation is based upon the *U.S. Standard Atmosphere, 1976,* which is not isothermal. In the G model the inverse Burger number [$\epsilon = (f_0 L)^2/(g\kappa D)$] is a function of height to reflect changes in static stability ($\kappa = D\partial \ln\Theta/\partial z$) between the troposphere and stratosphere. Here L is a horizontal length scale, defined by setting $\epsilon = 1$ at the bottom. Another difference from Green is the use of a more realistic basic flow U; it has a maximum at the tropopause level $z = z_t$ (Fig. 1). The prescription of the static state is important because the vertical variations of P, Θ, T, and ρ (density) are dominated by the static component of the prescribed state [see Grotjahn (1979, 1980) for details]. Figure 1 depicts the vertical distribution of basic-state potential vorticity gradient $\partial Q/\partial y$ for the G model.

The upper boundary is located at 50 km. Because of the small density at that height, the amplitudes of the eddies decay greatly before reaching the top boundary (see Holton 1974), and the rigid lid creates little difference from a radiation condition at the top. Indeed, most solutions are virtually unchanged for any boundary position above 35 km (Grotjahn 1980). Exceptions are the very long waves that are not emphasized here.

Periodic boundary conditions in the longitudinal and meridional direction are used for simplicity. These conditions allow use of plane wave solutions. We choose zero meridional wavenumber. The effect of using other meridional wavenumbers is to change the value of absolute wavenumber α with respect to zonal wavenumber k.

The interior equation for the G model is as follows:

$$ik(U-c)\left\{\epsilon\frac{\partial^2\Psi}{\partial z^2}+\left(\Omega\epsilon+\frac{\partial\epsilon}{\partial z}\right)\frac{\partial\Psi}{\partial z}-\alpha^2\Psi\right\}+ik\Psi\frac{\partial Q}{\partial y}=\gamma\left\{\epsilon\frac{\partial^4\Psi}{\partial z^4}+\left(\Omega\epsilon+\frac{\partial\epsilon}{\partial z}\right)\times\frac{\partial^3\Psi}{\partial z^3}-\alpha^2\frac{\partial^2\Psi}{\partial z^2}\right\} \quad (3.1)$$

with the boundary conditions

$$ik\left[(U-c)\frac{\partial\Psi}{\partial z}-\Psi\frac{\partial U}{\partial z}\right]=-\frac{\delta}{\epsilon}\nabla^2\Psi+\gamma\frac{\partial^3\Psi}{\partial z^3} \quad \text{at} \quad z=0 \quad (3.2)$$

$$ik\left[(U-c)\frac{\partial\Psi}{\partial z}-\Psi\frac{\partial U}{\partial z}\right]=+\frac{\delta}{\epsilon}\nabla^2\Psi+\gamma\frac{\partial^3\Psi}{\partial z^3} \quad \text{at} \quad z=5. \quad (3.3)$$

By using one γ value in (3.1)–(3.3), we assume that the paramaterized vertical diffusion has the same coefficient for potential temperature as for momentum.

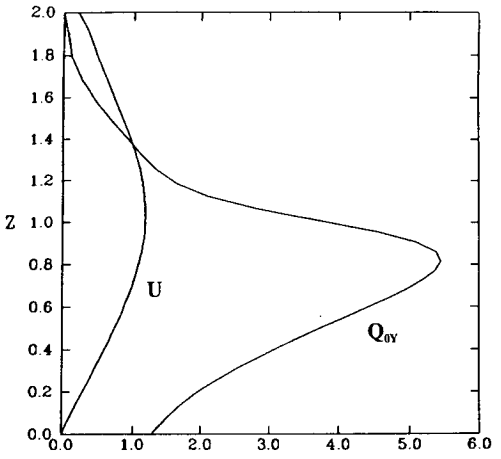

FIG. 1. G-model profiles of basic-state zonal wind, U, and potential vorticity gradient $\partial Q/\partial y$.

This amounts to choosing the turbulent Prandtl number to be unity as is standard.

The Eady model is recovered (i) for an f plane ($\beta = 0$), (ii) for isothermal conditions ($\epsilon = 1$), (iii) when inviscid ($\gamma = \delta = 0$), (iv) for U a linear function of height, and (v) when incompressible ($\Omega = 0$). Those assumptions cause $\partial Q/\partial y = 0$ and the equations above to be homogeneous. Our Eady model also lowers the top boundary to $z = 1$.

The system of equations is solved using centered difference schemes with 51 levels in the vertical direction to give a generalized matrix eigenvalue problem. Notice that the interior friction is related to, but is not equivalent to, the second derivative of q. As can be easily seen from (3.1), the most critical dissipative process in the interior is thermal conduction, which raises the order of the equation from second to fourth.

b. Implementing Ekman and interior friction

The governing equations include interior vertical diffusion in the momentum and potential temperature conservation equations. In addition, the usual Ekman layer friction is included; as is customary, each Ekman layer is "outside" the domain. Here γ is a coefficient that describes the interior friction due to second-order vertical diffusion, and δ measures the effect of boundary friction via the Ekman pumping. Terms multiplied by γ account for interior friction in the potential vorticity equation (3.1) and potential temperature equation. The potential temperature conservation equation is used to obtain boundary conditions (3.2) and (3.3). Ekman friction (the term multiplied by δ) comes from the same vertical diffusion term in the momentum equations as the γ terms, except the Ekman friction term results from a boundary layer analysis at the top and bottom. For positive relative vorticity, the lower boundary layer must include an upward flow out of the layer, while the

Unauthenticated | Downloaded 05/29/24 05:02 AM UTC

upper boundary layer preserves continuity with a downward flow. Hence, the sign of the δ terms is reversed in (3.2) and (3.3).

It should be recognized at this point that the problems we are addressing will be discretized. Because of this, the correspondence will be imperfect between the continuous spectrum eigenfunctions from the continuous formulation and the discrete spectrum with finite dimensional eigenvectors from the discrete formulation. However, it is only within the context of the discretized eigenvalue problem that such a correspondence can be made, and thus we limit ourselves to this comparison. With regard to the continuous problem, the correspondences that we examine may be viewed as comparisons of differing representations of the discrete spectrum of the viscous problem with differing amounts of (finite) dissipation. While this is artificial in the context of inviscid fluid flow, these examples of the effect of dissipation are pedagogically useful for the study of the initial value problem in Part II.

In the usual quasigeostrophic system, vertical diffusion is more than an order of magnitude larger in the Ekman boundary layer than in the interior of the domain. However, the sharp spike in the potential vorticity vertical structure of the inviscid continuum modes means that the vertical diffusion terms cannot be neglected for those modes because the viscous modified potential vorticity vertical scale can allow an order unity contribution by the interior vertical diffusion term. We now show that the vertical scale of potential vorticity for a "viscous-modified continuum mode" is proportional to $\gamma^{1/3}$.

Let $\eta = (z - c)\gamma^{-\chi}$, substitute it into (3.1), and rearrange to get

$$ik\gamma^{3\chi}\eta q' = \gamma \frac{\partial^2 q'}{\partial \eta^2}. \tag{3.4}$$

We can now determine what value of χ makes both sides of equal magnitude since γ is on both sides of (3.4). From (3.4), $\chi = 1/3$ and $\eta = (z - c)\gamma^{1/3}$. Let h be the vertical length scale of potential vorticity for a continuum mode near the critical level. Hence, $\eta \propto h$, and from (3.4), $hq' \propto \gamma q'/h^2$, which leads to $h \propto \gamma^{1/3}$ for a given wavenumber. This proportionality is reasonable because stronger viscosity would cause q to have a smoother shape and a larger length scale h. Also, vertical differencing requires $\Delta z < h/2 = 0.5\gamma^{1/3}$ in order to get physically correct *continuum mode* solutions when layers (or levels) are used. For midlatitude cyclones, $\gamma' = 3.6\ \mathrm{m^2\ s^{-1}}$ gives $\gamma^{1/3} \approx 0.12$ implying that at least 18 levels are needed to resolve the continuum modes when $0 \leq z \leq 1$.

Since the interior viscosity coefficient γ and Ekman friction coefficient δ are derived from similar terms, the proportionality between these two terms is unambiguous. Note that this is strictly true only if molecular viscosity is the damping mechanism. The coefficients may differ in a turbulent eddy diffusion parameterization. The values of δ and γ as well as their relationship are found by going through the scale analysis

$$\gamma = \frac{\gamma' L}{UD^2} = \frac{E_\nu}{2R_0}, \quad \text{where} \quad E_\nu = \frac{2\gamma'}{fD^2}$$

is the Ekman number, γ' is the eddy viscosity coefficient in dimensional form, and

$$\delta = \frac{E_\nu^{1/2}}{2R_0}.$$

The first feature to note here is that both γ and δ are related to E_ν; hence specification of the Ekman number specifies the interior viscosity coefficient too. Also $\delta = \gamma/E_\nu^{1/2} > \gamma$ as one might expect, because friction in the Ekman boundary layer exceeds interior viscosity. For the scaling choices used here, δ is 37 times larger than γ.

The eddy coefficient $\gamma' = 3.6\ \mathrm{m^2\ s^{-1}}$ has been used and it produces a relaxation time of 8.6 days. This γ' value represents a moderate Ekman friction, characteristic of a neutral boundary layer over open ocean or a stably stratified boundary over land (LP).

Once the interior friction term is added, (3.1) becomes a fourth-order ordinary differential equation and both (3.2) and (3.3) become third order. Obviously, numerical solution requires one more boundary condition each on the top and bottom in order to solve this problem using centered difference schemes. Therefore, another pair of consistent boundary conditions is needed. For the problem at hand,

$$\gamma\partial^2\Psi/\partial z^2 = 0 \quad \text{at top and bottom} \tag{3.5}$$

provides the extra boundary conditions. One can show that the matrix equation derived from the new boundary conditions will reduce to Eady's original equation when γ is set to zero, as it should.

The above equations and boundary conditions are derived for small Rossby and Ekman numbers with the Rossby number being order $E_\nu^{1/2}$ or less. The lower and upper boundary conditions are no slip for the velocity (applied as an effective Ekman pumping) and zero heat conduction for the temperature, which needs no boundary layer to effect. Note that some terms are retained that are small in scaling but can locally be important, such as the internal thermal conductivity.

4. Results

a. Eady model

In general, there are N eigensolutions for N grid points in the vertical. There is only one pair of amplifying/decaying normal modes for each wavenumber k. The other $N - 2$ solutions are neutral solutions with imaginary phase speed $c_i = 0$. Making Eady's assumptions, all solutions are neutral when $\alpha > 2.39994$, al-

Unauthenticated | Downloaded 05/29/24 05:02 AM UTC

though they include the so-called bottom-trapped and top-trapped neutral normal modes.

The continuum modes represent discrete sampling of a continuous spectrum of eigenvalues over the vertical domain. Figure 2 shows a continuum-mode structure ($\alpha = 2.0$) for the inviscid Eady model. Notice that a continuum mode does not seem to be a truly physical mode; the vertical structure of amplitude for a continuum mode has a kink at $z = c_r$. This kink causes a discontinuous vertical derivative; hence the q' profile for a continuum mode has a very sharp spike. Figure 3 illustrates the delta-function shape of continuum mode potential vorticity. Therefore, it is a basic property of the continuum modes to have a very small vertical scale and very large vertical derivatives. Because the interior viscous term has the highest differential order in the problem, it should be most important at the smaller spatial scales. A simple scaling argument, given above, shows that the vertical scale of potential vorticity for a continuum mode is proportional to $\gamma^{1/3}$, where γ is the interior vertical diffusion coefficient. Hence, for continuum modes the interior viscosity term has the same (or greater) magnitude as the Ekman pumping boundary condition has upon normal modes.

Friction reduces the maximum growth rates of the normal modes. When only Ekman friction is included, the decrease in growth rate is largest for α between 1.4 and 1.8 as well as for α beyond 2.4. In the interval $0 < \alpha < 2.3$, the growth-rate reductions range from about 0.03 to 0.11, and the maximum reduction occurs at about $\alpha = 1.6$. In the interval $2.4 < \alpha < 3.5$, where neutral normal modes occur in the inviscid case, all growth rates in the viscid cases become negative and the reduction in growth rate is about 0.2 or larger. Between $\alpha = 2.3$ and 2.4, the original positive growth rates change rapidly and become negative. It is not surprising to see that for normal modes with full friction,

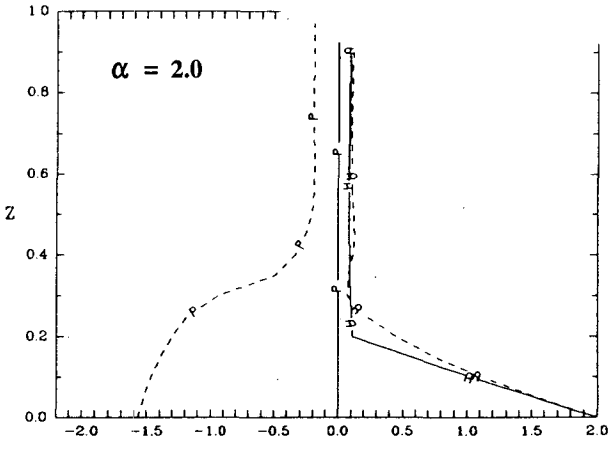

FIG. 2. Vertical profiles of streamfunction amplitude (A) and one-half phase angle (P) for a "lower-level trapped" Eady continuum mode in the two cases: inviscid (solid line) and Ekman plus interior friction (short dashed line).

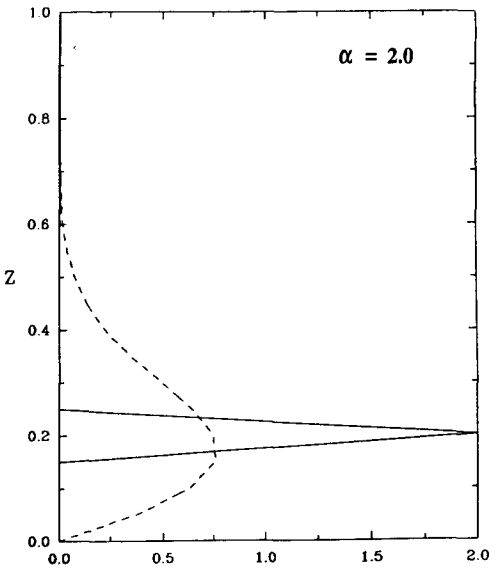

FIG. 3. The potential vorticity amplitude vertical distribution with height for two cases shown in Fig. 2: Ekman-only friction (solid line) and Ekman plus interior friction (short dashed line).

the growth rate spectrum is little altered from the case with only Ekman friction. The reason is simply that the vertical structures of normal modes change very smoothly with height; therefore the vertical diffusion in the interior is so small that one might simply ignore it.

The *continuum modes* have neutral (zero) growth rate for the inviscid and Ekman friction cases. In contrast, the Ekman plus interior friction case shows greatly reduced growth rates for all wavenumbers. The reduction in growth rates increases with wavenumber, α almost linearly. At $\alpha = 3.5$ the least damped mode decays at rate -0.42. (This may be contrasted with normal-mode growth rates that never exceed 0.3 in any case studied.) All the other continuum modes have an even larger negative growth rate for the full friction case.

The ability to make a one-to-one correspondence between continuum modes and their viscously augmented counterparts depends upon our use of rather coarse numerical vertical resolution (51 levels). (However, in comparison to state-of-the-art numerical models of the atmosphere, our resolution could hardly be termed coarse.) The use of such resolution allows us to identify individual modes within the continuous spectrum as interior viscosity and thermal conductivity become important. At higher numerical resolution, this is no longer possible, as continuum modes are singularly perturbed in their structure as the damping decreases and individual continuum modes are made up of a superposition of many viscously perturbed modes (Lin 1961). However, our argument remains intact in this case since all of the singularly perturbed modes have

Unauthenticated | Downloaded 05/29/24 05:02 AM UTC

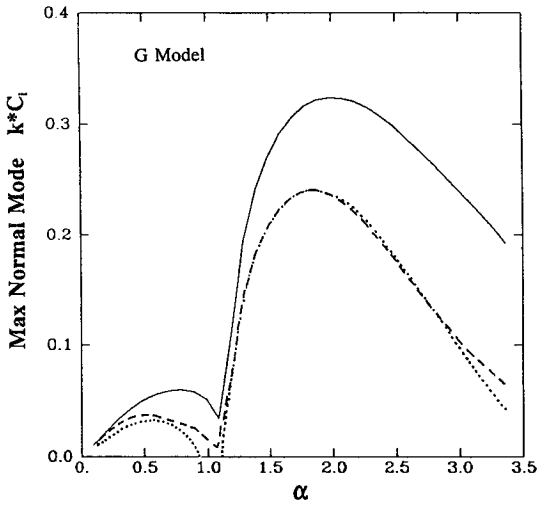

FIG. 4. The G-model normal mode maximum growth rate spectra for three cases: no friction (solid line), Ekman friction (dashed line), and Ekman plus interior friction (dotted line). When friction is present, $\gamma' = 3.6\ m^2\ s^{-1}$.

large damping rates. In fact, the decay rates for the singularly perturbed modes are uniformly larger than for modes to which a one-to-one correspondence can be made.

The amplitude distribution of streamfunction Ψ for a normal mode is slightly reduced by the inclusion of Ekman friction but is not affected by the addition of interior friction.

Figure 2 shows the amplitude of streamfunction Ψ for a lower-level-trapped continuum mode at $\alpha = 2.0$ for both inviscid and full friction cases. In the inviscid and Ekman friction cases, the vertical profiles for other continuum modes look similar, except that the "kink" occurs at different elevations. However, when interior friction is included there are two basic types of continuum-mode structures in the Eady model. Some look similar to the inviscid structures, while others have a single isolated maximum in the interior coupled with very large downstream tilt. The vertical structure of the continuum modes is unchanged by including only Ekman friction. The "kink" appearing in the inviscid case is smoothed by the interior friction. Instead of a constant phase angle as a function of height when there is no interior friction, Ψ for interior friction develops an eastward tilt. The eastward tilt is consistent with the damping of the continuum modes due to interior friction.

Figure 3 presents the distribution of potential vorticity for the same "lower-level trapped" mode with the cases having Ekman friction only and both friction terms as in Fig. 2. The inviscid case has the same shape as that of Ekman friction only. The delta-function shape of the inviscid and Ekman-only cases is smoothed out in the full viscosity situation; the flattening of the sharp peak (and removal of the kink in amplitude) has a more physically intuitive appearance for those modes that look like the inviscid solutions. However, the full viscosity solutions having a single interior peak amplitude do not look realistic due to the very large tilt.

b. G model

The maximum growth-rate spectra are plotted in Fig. 4 for *normal modes.* Instability extends to all wavelengths. The maximum growth rate is near $\alpha = 2$ in the inviscid case, corresponding to a dimensional wavelength of 4500 km. When Ekman friction is added, growth rates are damped in the whole spectrum. Since Ekman friction is proportional to vorticity, which in turn increases as wavenumber squared, the damping is proportionally larger as k increases. Whereas the Eady model shows little difference between the Ekman friction case and the full friction case, the two viscid cases in the G model are noticeably different in the growth rate spectra. The growth rate is smaller in the full friction case in the long- and short-wave ends of the spectrum. The growth rates are almost the same in the middle wavelengths.

Figure 5 displays plots of the growth rate spectra for G model *continuum modes* in the three cases; the interesting difference from the Eady model in this figure is that the Ekman friction actually slightly destabilizes the flow relative to the inviscid case in the G model, especially for the short waves. The destabilization is linked to the Ekman friction in this case because the

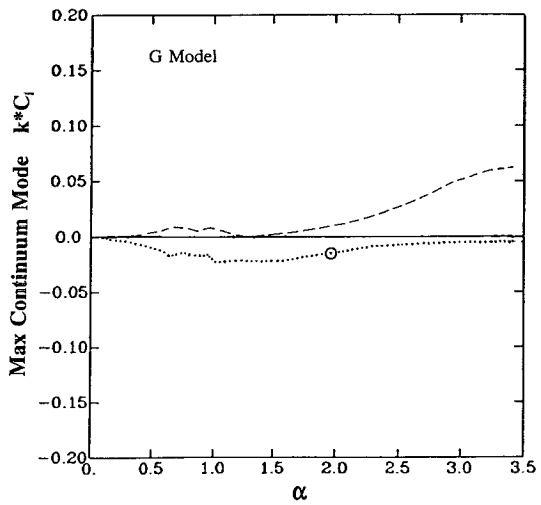

FIG. 5. The G-model continuum-mode maximum growth rate spectra for three cases: no friction (solid line), Ekman friction (dashed line), and Ekman plus interior friction (dotted line). The streamfunction amplitude of the mode with the growth rate indicated by the "⊙" is shown in Fig. 6b with a dot–dashed line. Growth rates for other modes shown in Fig. 6b are −0.102 for the dotted line mode; −0.496 for the solid line, dipole mode; and −0.490 for the dashed line mode. The mode shown in Fig. 7 has growth rate −0.67. Tropospheric continuum modes are heavily damped by the interior friction.

Unauthenticated | Downloaded 05/29/24 05:02 AM UTC

destabilization disappears when the lower boundary Ekman friction term is removed. One might expect that the upper Ekman layer has very little influence on the solution, since the upper boundary is placed at 50 km in the G model. This is further confirmed by calculating (nearly zero) growth rates when the Ekman layer is only at the top.

The explanation for this slight destabilization of a continuum mode may be given by invoking baroclinic energy arguments. First, multiply the linearized potential vorticity equation by $\rho_s\Psi'$ and integrate over the entire domain of the flow. Second, use the vertical boundary conditions

$$\left(\frac{\partial}{\partial t} + U\frac{\partial}{\partial x}\right)\frac{\partial \psi'}{\partial z} - \frac{\partial U}{\partial z}\frac{\partial \psi'}{\partial x} = \pm\frac{\delta}{\epsilon}\nabla^2\psi'$$

at $z = z_t$ and z_b and then apply zonal averages. One obtains the energy equation for the perturbation motion:

$$\frac{\partial}{\partial t}\iint \rho_s\left\{\frac{1}{2}[(\nabla\psi')^2] + \frac{1}{2}\epsilon\left[\left(\frac{\partial\psi'}{\partial z}\right)^2\right]\right\}dydz$$

$$= \iint\left(\rho_s\epsilon\frac{\partial U}{\partial z}\left[\frac{\partial\psi'}{\partial x}\frac{\partial\psi'}{\partial z}\right]dydz\right.$$

$$- \delta\left\{\rho_s\int\left[\left(\frac{\partial\psi'}{\partial x}\right)^2 + \left(\frac{\partial\psi'}{\partial y}\right)^2\right]dy\right\}_{z=z_{\text{bottom}}}$$

$$\left. - \delta\left\{\rho_s\int\left[\left(\frac{\partial\psi'}{\partial x}\right)^2 + \left(\frac{\partial\psi'}{\partial y}\right)^2\right]dy\right\}_{z=z_{\text{top}}}\right. . \quad (4.1)$$

The integrand on the left-hand side is the sum of the perturbation kinetic and available potential energy whose time rate of change is given by a sum of the three energy transfer terms on the right-hand side. Since the basic-state current U varies only with the height, the only source of energy for the growing disturbances is the zonal available potential energy. The conversion of the zonal available potential energy to eddy available potential energy is determined by northward heat flux. The first term on the right-hand side represents this baroclinic energy conversion. The remaining terms represent the sink of perturbation energy due to frictional dissipation in the lower and upper Ekman layers. In order to understand Fig. 5, the terms in (4.1) are calculated by using the eigenvector and eigenvalue for the "most unstable continuum mode" in the G model with Ekman friction only. It is found that by adding Ekman layers, a phase shift between v' and T' is created; the eddy heat flux created makes the baroclinic energy conversion term positive instead of zero as for the inviscid case. The boundary terms in (4.1) act to reduce the growth of the total energy, but their magnitude is much smaller (4 or 5 times smaller) than that of the baroclinic conversion term. Therefore, the inclusion of an Ekman layer in the G model can result in a net positive contribution to the total energy growth rate for some continuum modes.

In Fig. 5, growth rates are negative in the case having full friction, as in the Eady model. The magnitude of the plotted growth rates are much smaller than those for the full friction case in the Eady model. However, note that we are plotting the continuum mode that is least damped for each α here. In the G model, these least-damped modes have nonzero amplitude only at high levels. An example shown in Fig. 6b depicts the amplitude of the mode at $\alpha = 2$ corresponding to growth rate $kc_i = -0.0068$ and marked on Fig. 5 with the open circle. The amplitude of this mode is uniformly zero until above $z \approx 2.5$ (dimensionally above 25 km). Higher up, this mode has relatively large amplitude.

A brief explanation for the very small growth rate of such a mode is that at high levels the atmospheric density and Ω are very small; ϵ is also very small at high levels. Small Ω and ϵ lead to a smaller effect from the interior friction term [cf. Eq. (3.1)]. Therefore, the coefficients multiplying the highest derivative terms are very small at levels where an "upper level" mode would have significant amplitude, and vice versa. Only continuum modes with *negligible* amplitude in the troposphere show such small damping, but only continuum modes with *large* amplitude in the troposphere can be relevant to cyclogenesis.

Figure 7 shows the amplitude of a representative continuum mode having significant amplitude in the troposphere for $\alpha = 2$ in the three cases. The growth rate of this single-peak mode with full friction has large negative value and is well below the range used in Fig. 5. As one would expect, this "tropospheric" mode has much larger negative growth rate than that of the "upper level" modes. The same holds true for the other tropospheric modes (solid and dashed lines) shown in Fig. 6b. The numeric values of growth rates are given in the captions of Figs. 6b and 7.

The amplitude profiles for normal modes in the two viscid cases are almost identical. As observed in the Eady model, interior friction has little effect upon the normal-mode amplitudes.

In contrast, recall that the inviscid solution has a "kink" in the Eady model continuum modes. The kink is found near the critical level where the continuum-mode phase speed equals the basic flow U in the Eady model. The continuum modes have a complex variety of structures in the G model. For many continuum modes, the kink (Eady model) has become a "cusp" in the inviscid G model; that is, Ψ' has a very sharp peak in the interior instead of a minimum. The precise locations of the peaks vary for different continuum modes. For example, in Fig. 2 the kink is at $z = 0.2$; in Fig. 7 the cusp is at $z = 1.0$. The amplitude diminishes rapidly both above and below the cusp. Ekman friction makes little difference on the profile, as found

Unauthenticated | Downloaded 05/29/24 05:02 AM UTC

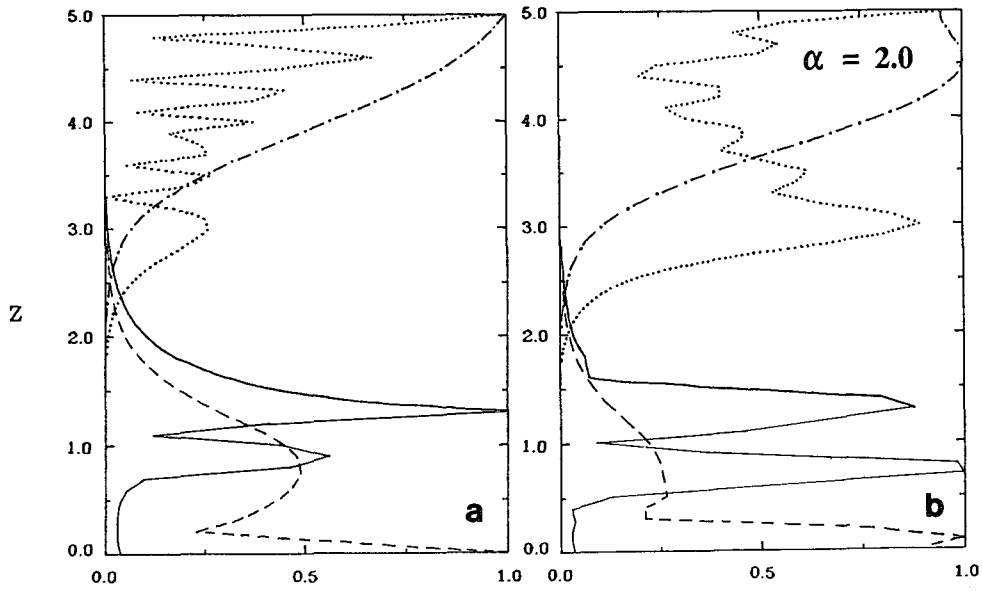

FIG. 6. Vertical profiles of amplitude for continuum modes in the G model. Representative examples of three classes are shown. (Figure 7 is a typical single-peak mode.) Upper-level modes (dotted and dot–dashed lines) are relatively insensitive to friction. Other modes are sensitive to interior viscosity (dipole modes: solid line) and (broad secondary maximum modes: dashed line). (a) Solutions without friction; (b) solutions with full friction. Growth rates of the modes in (b) are given in the previous caption.

before. By including the interior friction the cusp is smoothed, consistent with the Eady model result.

The continuum-mode structure is highly sensitive to the basic-state wind fields and other prescribed parameters such as ϵ and Ω. For this formulation of the G model, the continuum modes might be grouped into four categories. Representative structures for three of the categories are shown in Fig. 6. The types include (i) upper-level modes (many of which have multiple peaks in amplitude), (ii) single spikes in amplitude, (iii) double-spiked amplitude profiles with the maxima lying on either side of the maximum in U, and (iv) modes with a very sharp spike near the bottom along with a broader secondary maximum above. All of these modes, except for a few upper-level modes, have sharp peak amplitudes in their potential vorticity.

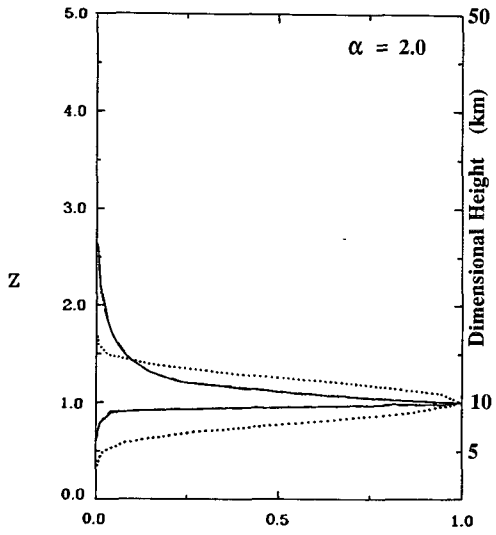

FIG. 7. A representative single-peak continuum mode in the G model. Vertical profile of streamfunction amplitude is plotted for inviscid (solid line), Ekman friction only (dashed line), and full friction (dotted line). The growth rate of the full friction mode shown is −0.67; the other two modes are neutral and virtually identical.

One may compare the potential vorticity distribution of the same modes presented in Fig. 7 between cases with only Ekman friction and the case with full friction. For the case with Ekman friction only, the potential vorticity exhibits a single-spike profile, rising sharply to a maximum at around $z = 1.0$ (=10 km) followed by a steep decline. It is essentially zero above $z = 1.4$. In the full friction case, the sharp peak is smoothed and broadened. The results basically mirror the conclusions reached from the examination of the amplitudes in Fig. 7. The sharp peak amplitudes of q for other continuum modes are similarly smoothed and broadened, as well.

5. Conclusions

This report considers the effects of Ekman and interior friction upon two models of frontal cyclogenesis. The models are the Eady (1949) model and G model (Grotjahn 1980). The G model includes compressibility, variable Coriolis parameter, an interior maximum in basic-state wind field, and realistic static stability.

Unauthenticated | Downloaded 05/29/24 05:02 AM UTC

These models have two basic types of solution: normal modes and continuum modes. Most previous studies have emphasized the normal modes. Continuum modes are not damped by Ekman friction in the Eady model. However, the vertical structure of an inviscid continuum mode has a sharp kink or cusp in the streamfunction. (In contrast, inviscid normal modes have smooth vertical structure.) Hence, continuum modes respond to interior viscosity much more strongly than normal modes when interior viscosity is formulated using multiple vertical derivatives.

a. *Normal-mode results*

In the inviscid case, there are two normal modes for each wavenumber, one growing and the other decaying. For the Eady model, there is a short-wave cutoff to the instability. Beyond the critical absolute wavenumber $\alpha = 2.4$, no growing or decaying normal modes exist. The G model, on the other hand, does not have a short-wave cutoff. The G-model amplitude profile has maxima at the bottom and near the simulated tropopause. Ekman layer friction decreases growth rates compared to the inviscid case. In the Eady problem, long waves still have fairly large positive growth rates, while short waves are strongly damped for the reasonable eddy viscosity coefficient ($\gamma' = 3.6\ m^2\ s^{-1}$) used here. The G model's growth rates are also reduced noticeably but still remain positive for the wavenumbers of interest. In the case having full friction, solutions are almost identical to the case with the Ekman friction only, except for slight additional damping at the short- and long-wave ends in the G model. In both models, addition of interior friction does not have much effect on the solution.

b. *Continuum-mode results*

In the Eady model, all continuum modes are neutral by definition in the inviscid case, and the eddy quasi-geostrophic potential vorticity has a delta-function shape at the critical level. When Ekman friction is added, the solutions are almost identical to those in the case with no friction, since the eddy potential vorticity vanishes at the top and bottom boundaries in the Eady model. Some solutions in the G model, however, are slightly destabilized due to the lower Ekman layer. The upper Ekman layer plays little role in the G model because density is so small there. The full friction case shows negative growth rates for all continuum modes in both models. The most substantial damping occurs for continuum modes with amplitude peaks in the troposphere. For a small number of levels (e.g., 5) the continuum modes with full friction have *small* damping. But when the modes vertical structures are better resolved (as anticipated by our scale analysis) the negative growth rates rapidly increase for modes whose amplitude is significant in the troposphere. In addition, the rate of damping of the continuum modes shows a proportional sensitivity to the size of the interior viscosity coefficient; for example, when the interior viscosity coefficient is reduced by one-third, continuum modes with tropospheric amplitude are damped roughly one-third as much.

The complete friction has two effects on the continuum mode's structure. 1) The very sharp changes in the potential vorticity profile are smoothed out, so the structure has a more physically sensible appearance in G and some Eady model solutions. 2) The meaningful continuum modes become strongly damped. In the G model some continuum modes are weakly damped for the full friction case, but they are not meaningful to cyclogenesis because they only have amplitude in the high stratosphere. These results confirm our hypothesis that interior friction has a much more profound effect on the continuum modes than on normal modes. Therefore, it is necessary to include interior friction when one considers frictional effects upon continuum modes.

Finally, the structure of the continuum-mode analog solutions in the G model differ from those in the Eady model in an important way. Continuum modes in the inviscid Eady model have nonzero amplitude over a considerable depth (often the entire depth). In contrast, the amplitude profiles of individual continuum modes have much less overlap in the G model. As discussed in Part II, having overlap in vertical amplitude may increase a nonmodal form of amplification.

Acknowledgments. This report is based upon the master's thesis of the second author. The research was supported in part by National Science Foundation Grant ATM 86-06267 (until 2/90). The work was completed using University of California Hatch Grant ID 7712 funds.

REFERENCES

Barcilon, V., 1964: Role of the Ekman layers in the stability of the symmetric regime obtained in a rotating annulus. *J. Atmos. Sci.*, **21,** 291–299.

Bretherton, F. P., 1966: Critical layer instability in baroclinic flows. *Quart. J. Roy. Meteor. Soc.*, **92,** 325–334.

Card, P. A., and A. Barcilon, 1982: The Charney stability problem with a lower Ekman layer. *J. Atmos. Sci.*, **39,** 2128–2137.

Charney, J. G., 1947: The dynamics of long waves in a baroclinic westerly current. *J. Meteor.*, **4,** 135–162.

Eady, E. T., 1949: Long waves and cyclone waves. *Tellus,* **1,** 33–52.

Farrell, B., 1985: Transient growth of damped baroclinic waves. *J. Atmos. Sci.*, **42,** 2718–2727.

Green, J. S. A., 1960: A problem in baroclinic instability. *Quart. J. Roy. Meteor. Soc.*, **86,** 237–251.

Grotjahn, R., 1979: Cyclone development along weak thermal fronts. *J. Atmos. Sci.*, **36,** 2049–2074.

——, 1980: Linearized tropopause dynamics and cyclone development. *J. Atmos. Sci.*, **37,** 2396–2406.

Holopainen, E. O., 1961: On the effect of friction in baroclinic waves. *Tellus,* **13,** 363–367.

Holton, J. R., 1974: On the trapping of unstable baroclinic waves. *J. Atmos. Sci.*, **31,** 2220–2222.

Unauthenticated | Downloaded 05/29/24 05:02 AM UTC

Lin, C. C., 1961: Some mathematical problems in the theory of the stability of parallel flows. *J. Fluid Mech.,* **10,** 430–438.

Lin, S.-J., and R. Pierrehumbert, 1988: Does Ekman friction suppress baroclinic instability? *J. Atmos. Sci.,* **45,** 2920–2933.

Miles, J. W., 1965: Effects of diffusion on baroclinic instability of the zonal wind. *J. Atmos. Sci.,* **22,** 146–151.

Pedlosky, J., 1987: *Geophysical Fluid Dynamics.* Springer-Verlag, 710 pp.

Phillips, N. A., 1954: Energy transformations and meridional circulations associated with simple baroclinic waves in a two-level quasi-geostrophic model. *Tellus,* **6,** 273–286.

Romea, R. D., 1977: The effects of friction and β on finite amplitude baroclinic waves. *J. Atmos. Sci.,* **34,** 1689–1695.

U.S. Committee on Extension to the Standard Atmosphere, 1976: *U.S. Standard Atmosphere 1976.* U.S. Govt. Printing Office, 227 pp.

Williams, G. P., and J. B. Robinson, 1974: Generalized Eady waves with Ekman pumping. *J. Atmos. Sci.,* **31,** 1768–1776.

Unauthenticated | Downloaded 05/29/24 05:02 AM UTC